SEGMENTED HEXAGONAL ANTENNA REFLECTOR CONCENTRICALLY STACKED USING SHAPE MEMORY COMPOSITE TUBULAR HINGES

Juan M. Fernandez[(1)], Andrew F. Paddock[(1)], Kevin S. O'Neal[(2)], Kevin Demarco[(2)]

[(1)]NASA Langley Research Center
Hampton, VA 23681, U.S.A.
Email:juan.m.fernandez@nasa.gov

[(2)]Analytical Mechanics Associates, Inc.
NASA LaRC, Hampton, VA 23681, U.S.A

Abstract

A new architecture for solid surface reflector antennas scalable to sizes greater than 10 m is presented. The design combines the compact, lightness and simplicity characteristics of advanced deployable structures to create sub-reflectors that can be assembled in space into larger units using a robotic arm and operations under development by a related parallel project. The seven-panel hexagonal sub-reflector is divided into hexagonal panels of that efficiently stack concentrically and vertically. The central panel is connected to each side panel on the back side by a pair of tubular shape memory composite hinges that enable the required deployment kinematics. A secondary mechanism ultimately closes the interpanel gap. The focus of the paper is on the development of the sub-reflector elements, namely the tubular hinges that use embedded heaters and sensors for actuation, the actuation mechanisms, and the lightweight sandwich construction panels. A finite element analysis parametric study was conducted to assess how design features of the hinge affect its stowage and deployment dynamics. The component fabrication and testing plans for the two-panel assembly breadboard model are outlined.

I. INTRODUCTION

Fixed solid surface reflector antennas are normally constructed up to a diameter of 4 m due to the size of launch vehicle fairings. Given their high surface accuracy and low transmission losses, they can target higher radio frequencies than deployable mesh or membrane reflectors, which are more scalable in nature. To increase volumetric packaging efficiency, several efforts have targeted deployable solid surface reflectors. However, in general, those designs have been limited in size to less than 10 m diameters due to high mass and mechanical complexity. The typical architecture is to have a central hub that is surrounded by a series of petals or gores supported on a deployable metering structure. The traditional approach is for these petals to be rigid, and thus such reflectors require a high degree of mechanical complexity to stow and deploy to the required accuracy, normally following a wrap-rib or radial and axial hinge approach for the backbone support structure [1]. Researchers have investigated advanced designs that make use of deformable thin-shell composites reflective surfaces made from low-thermal expansion, high-strain carbon fiber composite materials that allow the entire reflector to stow more efficiently by elastically deforming the material [2-3]. Advanced concepts that involve in-space assembly (ISA) [4], and even most-recently spacecraft formation flying have been proposed to scale up the reflector surface [5]. Maxar Technologies will be demonstrating circa 2024 as part of the National Air and Space Administration (NASA) On-orbit Servicing, Assembly, and Manufacturing (OSAM-1) mission the in-space assembly of a 3-m antenna reflector from seven 1-m size hexagonal rigid panels, which will be fixed to one spacecraft facet [6]. Assembly of each side panel one by one to the central panel attached to the main spacecraft boom will be carried out autonomously by a 5-m-long robotic arm that locates and bolts down each panel. The payload called Space Infrastructure Dexterous Robot (SPIDER) will robotically assemble the communications antenna and demonstrate Ka-band radiofrequency (RF) transmission with a ground station on Earth.

A new collaboration effort was established in 2022 between NASA Langley Research Center (LaRC) and Maxar Technologies to study advanced packaging methods using flexible composite technology for the next generation of large, segmented, solid surface antenna reflectors compatible with in-space assembly by robotic arm operation. LaRC was tasked with developing an architecture and flexible composite substrate to simplify and reduce the number of robotic operations of scaled-up systems of SPIDER that would otherwise require multiple rings of hexagonal panels to enlarge the area of the aperture.

The architecture down selected as well as the design of the thermally and dimensionally stable composite substrate consists of sets of tubular composite hinges used to connect the backside of many rigid segments that form the large parabolic reflector, which for a larger version will be assisted by the robotic arm. The construction of the tubular hinges and hexagonal panels is presented in this paper, as well as the component level

testing and analysis carried out on the hinges to characterize their static and dynamic behaviors. The design of the two-panel (2/7th area) breadboard model demonstrator that will be used to assess and validate the new concept will also be shown. This system is designed to serve as a 3.3-m scale sub-reflector for a future 10-m diameter robotically assembled reflector. The final validation test campaign, followed by requirements compliance and concept feasibility assessment is expected in the last quarter of 2023.

II. Architecture Design

The use of a new shape memory composite (SMC) material with integrated heating and sensing capabilities was developed to reduce part count (complexity), power requirements, and cost of larger antenna reflectors, while enabling a high deployed stiffness solution with predictable and controlled deployment dynamics [7]. The deployable reflector uses these SMC hinges to connect and stack all hexagonal rigid panels stowed in a convex configuration under the central concave panel, as shown in Fig. 1 [8]. The initial concept produced a vertically staggered panel assembly configuration such that the SMC hinge would seamlessly mate the side panels with the central panel, without the need of a secondary closing mechanism. However, for a volumetrically efficient stowed configuration, where all side panels are stacked concentrically under the central one, a secondary spring-loaded mechanism is used to close the initial panel-to-panel gap left by the deployment of the composite hinges. Each pair of SMC hinges are anchored to each side panel by a carriage that translates along two side tracks or rails parallel to the hinge longitudinal axis. A mechanical reel that has a lanyard connected to a constant force spring provides the actuation force and necessary extension to close the inter-panel gap. A hold down mechanism in the form of a Frangibolt from TiNi Aerospace† secures the assembly for launch and until the pair of tubular SMC hinges have completed the initial rotation of the side panel, as shown in Fig. 2.

The outermost side panel (furthest from the central one) will connect to the spacecraft boom. As this panel deploys first, the stacked sub-reflector will be displaced from the spacecraft and the rest of the side panels will deploy one at time triggered by the thermally actuated SMC hinges. The final product is a series of high-precision sub-reflectors, each cantilevered from a small offset boom that the robotic arm will use to place and fix to the main central deployable sub-reflector already supported from the main spacecraft boom, as shown in Fig. 3. To increase the number of load paths through each sub-reflector and increase global deployed stiffness, the same type of Interconnect Assembly Plates used in the SPIDER demonstration in envisioned to secure additional side panels from the central and side sub-reflectors. The goal is to enable an architecture that does not require a longer robotic arm than the size of the central sub-reflector in order to keep cost down as the system scales up since the robotic arm is one of the main cost drivers.

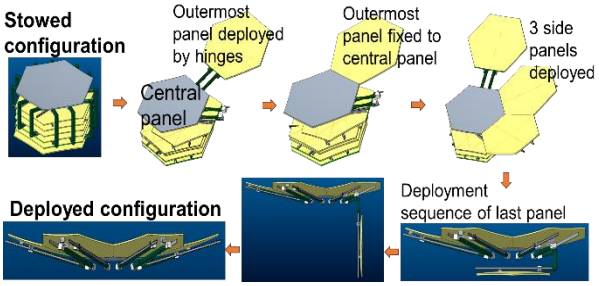

Fig. 1. Deployment sequence of a concentrically stacked seven-panel reflector by SMC hinges. Side panel deployment occurs one at a time from the outmost panel until all are fixed to the central panel.

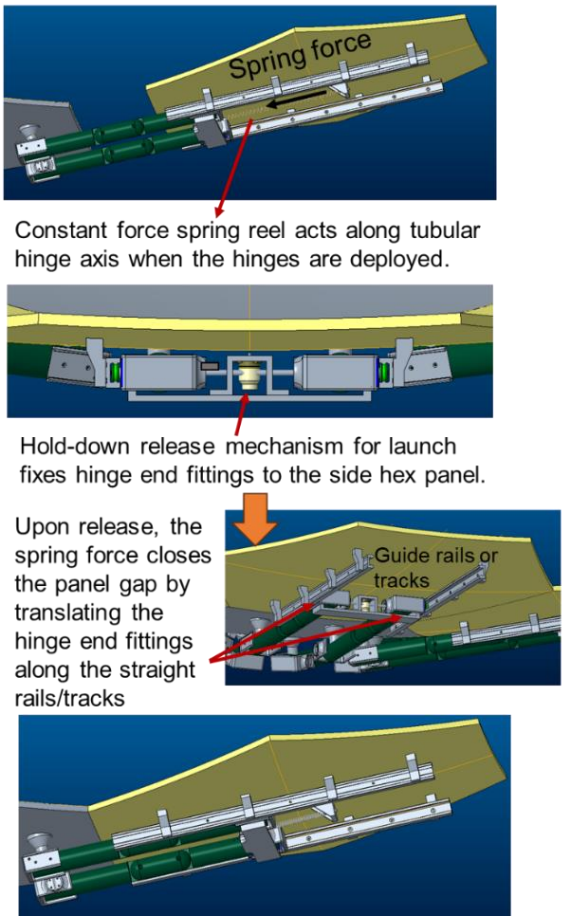

Fig. 2. Secondary spring-loaded mechanism to close the initial inter-panel gap left by the pair of hinges.

† Specific vendor and manufacturer names are explicitly mentioned only to accurately describe the analytical tools used. The use of vendor and manufacturer names does not imply an endorsement by NASA nor does it imply that the specified equipment is the best available.

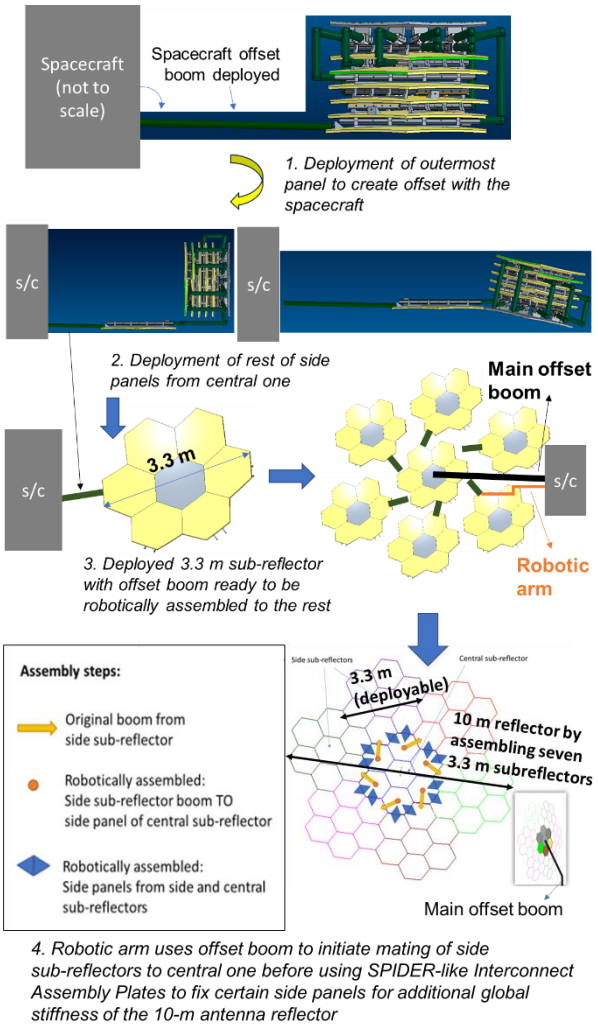

Fig. 3. Scalable architecture design using a combination of deployable and robotic arm in-space assembly. The figure shows the steps to construct a 10-m reflector.

III. Tubular Hinge Design and Analysis

The key technology that enables compact stowage of the numerous rigid panels in a concentrically stacked configuration is the composite tubular hinge. Each side panel is cantilevered from the central panel by a pair of hinges, and thus this deformable backbone structure needs to provide the dimensional and structural stability required for a precision reflector, as well as the flexibility to change the configuration of the system from packaged to deployed. Since the vertical offset of each side panel from the central one is different in the stack, every pair of hinges will have a unique geometry, as represented in the top image of Fig. 4. The hinges are composite tubes with a pair of diametrically opposite dogbone-shaped cutouts that enable localized pinching and folding the hinge without damage [9]. Dogbone slots are preferred over straight slots with a constant slot width to increase deployed stiffness and minimize the risk of hinge snap back and deployment anomaly [10]. The innermost panel in the stack will have a single pair of dogbone slots as the vertical offset from the neighbouring central panel is small. The rest of the five side panels will all have two pairs of dogbone slots separated a certain distance proportional to the vertical offset from the central panel they need to clear in the stacked state. Two different designs of single-slot hinge pairs for Side Panel #1 in the stack are shown in Fig. 4 (a). A longer two-slot hinge for Side Panel #2 is presented in Fig. 4 (b). These SMC hinges have integrated heaters for thermal actuation. The heater leads can be observed protruding from one of the hinge ends. Since the vertical offset of each unique hinge pair depends on the system level design of the reflector with factors such as minimum panel thickness, panel area, or secondary closing mechanism design, that are subject to change, it was necessary to understand the design space for the tubular hinges given a set of building-block features common in all designs.

(a)

(b)

Fig. 4. SMC hinges with integrated heaters and the same dogbone slot geometry: (a) single-slot hinge pairs with a tube diameter of 45 mm (left) and 38 mm (right); (b) two-slot hinge with a diameter of 45 mm.

A parametric study for a single-slot hinge was produced to assess how design features affect three critical performance metrics that allow down-selection:

1) Composite laminate strains in the folded state of the hinge.

2) The deployment moment-rotation relationship to determined steady-state and peak deployment moment to overcome snap back, as well as hinge deployed stiffness.

3) Whether the hinge snaps back at the end of deployment once an inertial tip mass equivalent to the side panel assembly is attached. The higher the dynamic peak moment the higher the locking moment, i.e. the moment that needs to be applied to start folding the hinge.

Three independent parameters were traded in the study: tube diameter, hinge slot length, and the diameter at the end of the dogbone slot (with the slot width being

proportional to it). Three different dimensions (small, medium and large) for the three independent parameters were used, as shown in Fig. 5. This hinge parametric study generated a total of 27 unique analysis cases.

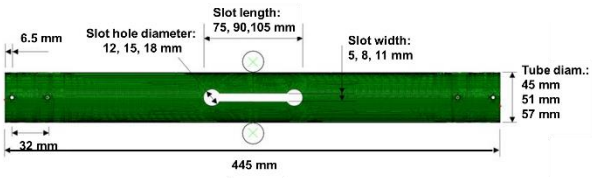

Fig. 5. Design parameters used in the trade study of the single-slot tubular hinge.

The finite element analysis (FEA) software Abaqus was used to simulate the quasi-static folding and deployment of the simple tubular hinge. One critical design parameter that affects the hinge response is how the hinge interfaces with the two panels it connects to. Tubular hinges with various end conditions were first analyzed to assess hinge stiffness, deployment moment-rotation behavior, and folding strains. These hinges all had a 45-mm diameter, 90-mm slot length, 15-mm slot hole diameter, and 8-mm slot width. This hinge design is considered the nominal case and was used for manufacturing trials. The hinge ends were either: a) completely free; b) restrained partially by a pair of soft springs that connect sections diametrically-opposite; c) completely restrained to the initial circular shape by internal plugs; d) or, as shown in Fig. 6, by two pairs of rods that connect sections diametrically-opposite. The bending test fixture presented is being used to measure the quasi-static deployment moment-rotation relationship of these SMC hinges and correlate with the FEA. Motors driving the hinge ends using a gear and lead screw rotate the ends in steps by equal amounts while the torque sensors in line with the rotation axis measure the self-deployment moment of the hinge. Different hinge end conditions are being investigated using this test fixture.

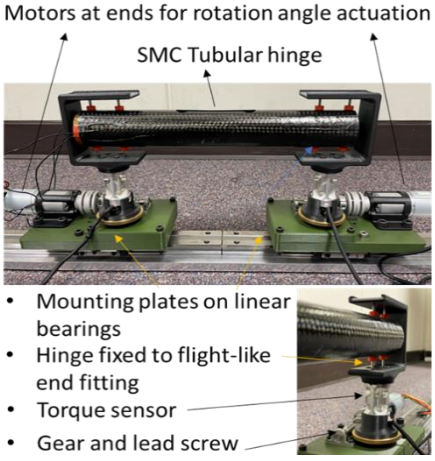

Fig. 6. Bending test fixture with representative hinge ends boundary conditions for moment-rotation relationship measurement.

The analyses determined that the plugged-end condition was too stiff to allow this design to fold beyond a total 135º hinge rotation, producing high folding strains and a high peak moment ~2.3x larger than the other cases. The case with the free ends showed the lowest folding strains, as the ends could ovalized completely, but produced the lowest deployed stiffness. The cases with the partially-constraint ends either by soft springs or two parallel rods presented a compromise between folding strains and deployed stiffness and had similar peak moments as the free-ends case. It was decided to use the two parallel rods option as a simpler approach to implement physically, so all subsequent simulations, including the parametric study, used these boundary conditions.

For the parametric study of the single-slot hinge, the quasi-static folding was carried out by first pinching the slots together using two 25-mm diameter mandrels. Then, opposing rotations to the ends were prescribed to begin folding the pinched hinge. The two mandrels were removed when the hinge was partially folded, and the analysis continued until the tube ends met with the hinge fully folded about 180º. The strain field in the stowed state were recorded. The maximum principal strains in the folded condition of all 27 hinge design cases simulated are presented in Fig. 7. The peak compressive strains are normally around the ends of the slots. Several conclusions can be drawn from this graph. First, it is surprising to find that in most cases, the growth in the diameter of the hole is inversely proportional to the maximum compressive strain, except for certain cases with a small slot length. Removing more material at the ends of the slot is effective if it does not impact the arc length needed to fold the tube. Second, folded strains diminish with both the tube diameter size and the slot length. Finally, folded strains between 1.2% to 2.2% are expected, suggesting the use of intermediate modulus carbon fiber laminates with high strain to failure.

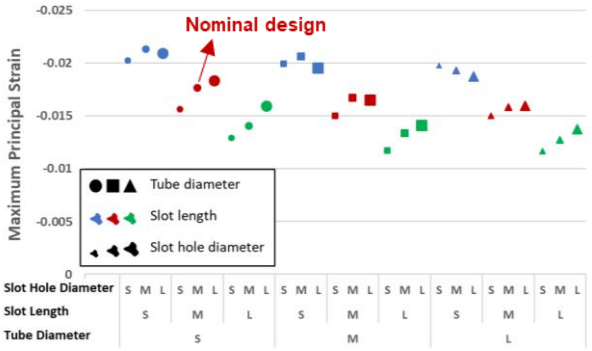

Fig. 7. Maximum strains obtained in the folded state of the hinge for all 27 design cases from combining the three independent design parameters (tube diameter, slot length, and slot hole diameter) at the different sizes: small (S), medium (M), and large (L). The nominal hinge design is also highlighted.

For the deployment phase, three types of analyses were carried out. First, a quasi-static deployment step by prescribing equal rotations on both ends of the tube was performed until the hinge started to snap through and then the quasi-static simulation was completed using a dynamic solver. This approach provided the deployment moment-rotation graph shown in Fig. 8.

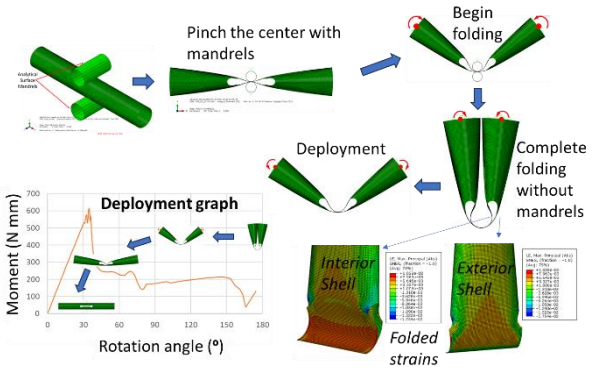

Fig. 8. Analysis steps to quasi-statically fold and deploy the single-slot hinge. The folded hinge strains in the interior and exterior shells around the slots are shown, as well as the deployment moment-rotation graph with a 200 N-mm steady-state moment until snap-through at a 600 N-mm peak moment at a total 35º rotation angle.

The second approach was a dynamic deployment simulation where at one end of the hinge the same boundary conditions at the end of the folded state were kept (fixed), while at the opposite end the constrain on the rotation axis was released. The goal of this dynamic case was to assess if the hinge snapped back to the straight configuration or not. Three of the hinge designs analysed did not achieve a complete deployment. These cases all had the large size tube diameter of 57 mm combined with the small size slot diameter hole of 12 mm and slot width of 5 mm. The slot length size did not make a difference. The inside of the folded tube did not recover fully during deployment and forced the hinge to either backlash or snap back, as shown in the rightmost image of Fig. 9 (a). It is believed that the smaller diameter tubes with the larger slots the shell ligaments near the slots subtend a smaller arc length and thus are more flexible. The three cases that did not finish straight are more energetic than the ones with larger slots. The base moment-rotation graph for the nominal case is shown in Fig. 9 (b). Three moment peaks of increasing magnitude before the hinge fully snaps through are visible. The first peak at a 90º rotation angle is minor and corresponds to the folded ligaments slightly traveling axially and rearranging their configuration. The second peak at a 30º remaining angle corresponds to snap though of the outer ligament. The third peak, which is the most energetic one, at a 6º angle corresponds to the snap through of the inner ligament.

After the hinge recovers its straight configuration, the tube continues to vibrate back and forth about the 0º angle producing very high moments of 7 Nm – 10 Nm at the base until the kinetic energy dissipates. The dynamic deployment sequence of a hinge with the nominal design dimensions is shown in Fig. 9 (c). The SMC hinge was actuated by the embedded heaters and self-extended to the final straight state with a deployment path that matched the simulation.

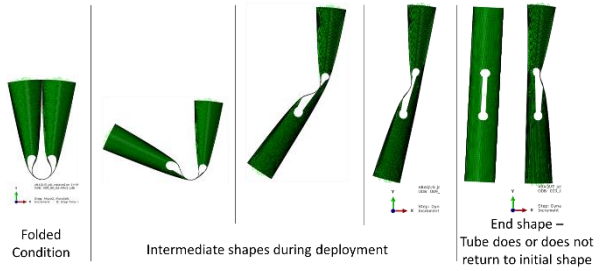

(a)

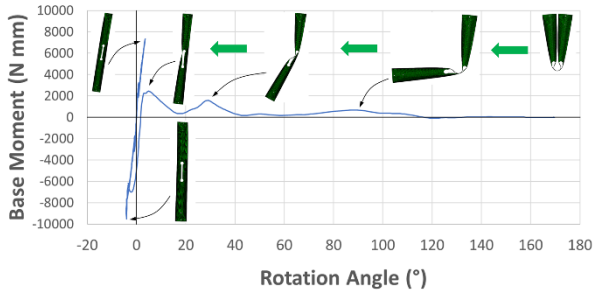

(b)

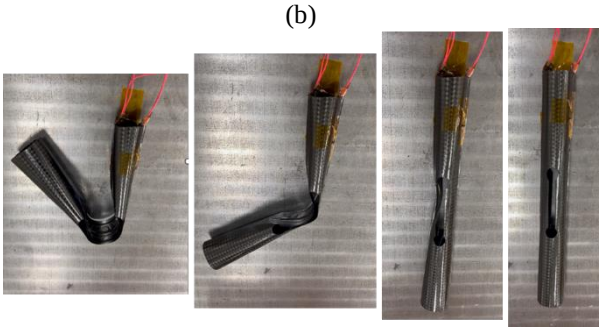

(c)

Fig. 9. Dynamic deployment steps of the hinge without a tip mass attached to the moving end. (a) The simulated end shapes on the right show two different cases: one where the tube has returned to the straight configuration, and one where the tube has snapped-back into an unwanted end state; (b) deployment moment-rotation relationship graph showing final moment peaks when the hinge snaps through; (c) Test article deployed using the embedded heaters and locking into the final straight configuration.

A third dynamic simulation approach followed the same boundary conditions as for the second approach but a 4.15-kg mass fixed to the moving end of the hinge and located at the center of gravity (CG) of the side panel assembly. The inertial mass was half the total mass of the panel assembly since a single hinge was

simulated, and to prevent unrealistic twist from the asymmetric configuration, the CG was aligned with the axis of the hinge. The objective was to assess potential snap-back at the end of the deployment due to the inertial mass.

A parallel study on the SMC plain weave laminate determined that the hinge material when bent uniformly above its glass transition temperature (Tg) of 120ºC could experience tow microbuckling and kinking at a folding radius < 20 mm. In general, this leads to some delamination in the compression side of the kinked region. However, the deformation did not lead to loss of shape recovery unless tow/fiber/resin fracture was present, which was experimentally determined to occur at a folding radius < 6 mm. For the maximum 0.22-mm wall thickness of the laminate at the region where the heaters are present, this results in a not-to-exceed surface compression strain of 1.83%. The nominal hinge design shows a maximum strain level of 1.78%, as reported in Fig. 8, and although no damage has been visually observed on the specimens tested, it is believed that the design is marginal against failure. A longer slot length would reduce the strain level around the slot end and should be considered in a future design iteration.

The next step in the analysis process involved the assessment of the folding and deployment behavior of a two-slot hinge. A FEA of the quasi-static folding of a single hinge from Side Panel #2 is presented in Fig. 10. This hinge was previously shown on Fig. 4 (b). Achieving a folded state that matched the desired configuration needed in the panel stack, which result in a rotation angle of 92º for one end and 100º for the other end, required multiple steps. First, effectively pinching the two slots required two pairs of mandrels moving synchronously. Then, the two lines of nodes between mandrels were pinned while the mandrels were moved out. Using several cycles of partial rotation between the left and right side of the hinge while one set of nodes was pinned, and the other set was released was necessary to complete the rotation of the hinge ends into the desired relative angles. The dynamic deployment study under this configuration is ongoing.

IV. FABRICATION AND TESTING

The new reflector architecture proposed required fabrication advancements on several areas to produce parts with the required thermal and dimensional stability characteristics. The tubular hinges require integrated heaters for actuation of the SMC material, as well as embedded temperature sensors for closed-loop control and strain sensors to confirm deployment. The Pennsylvania State University (PSU) developed for this project custom ultrathin-film heaters to NASA specifications. They are produced using microfabrication and have a total thickness of 25 µm: 12-µm polyimide substrate, 9-µm copper active layer, and 4-µm polyimide encapsulation. The heaters have the dogbone slots and multiple units are joined by microfabricated leads to yield an integrated part that can be embedded directly into the laminate stack, as shown in Fig. 11. The lead ends protrude outside of the SMC hinge so that electrical connections with the rest of the hardware can be made. Temperature uniformity tests at the minimal operational temperature of 125ºC were carried out prior to assembly. Under room temperature conditions, each heater unit requires 22 W of power to reach the minimum operational temperature. For the single and two-slot hinge this translates to about 44 W and 88 W of power to actuate the hinge for about 10 s to 15 s. Some of the steps of the fabrication process of the SMC hinge is shown in Fig. 11.

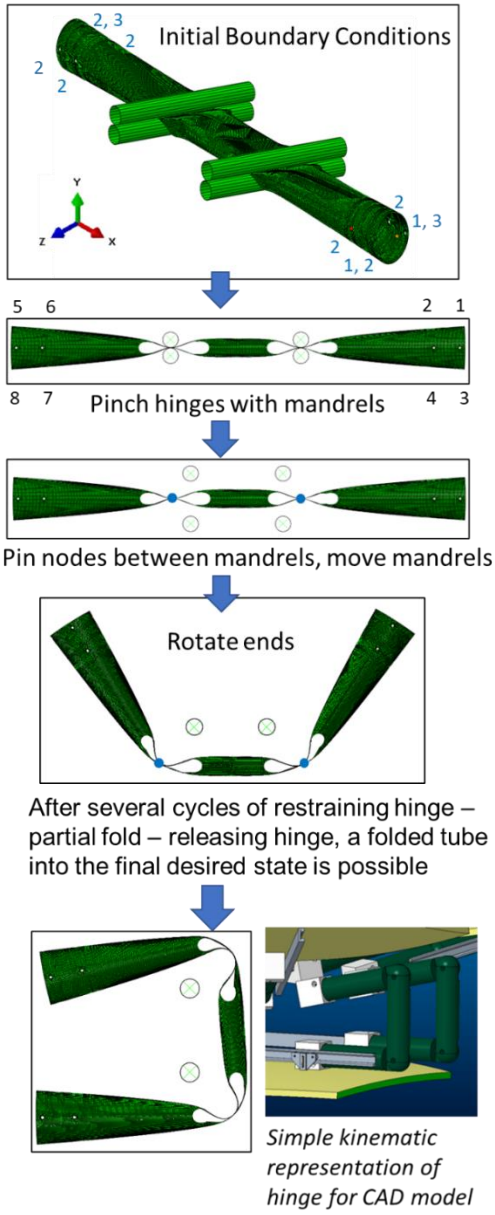

Fig. 10. Quasi-static folding a two-slot hinge into the desired stowed configuration for subsequent dynamic deployment study.

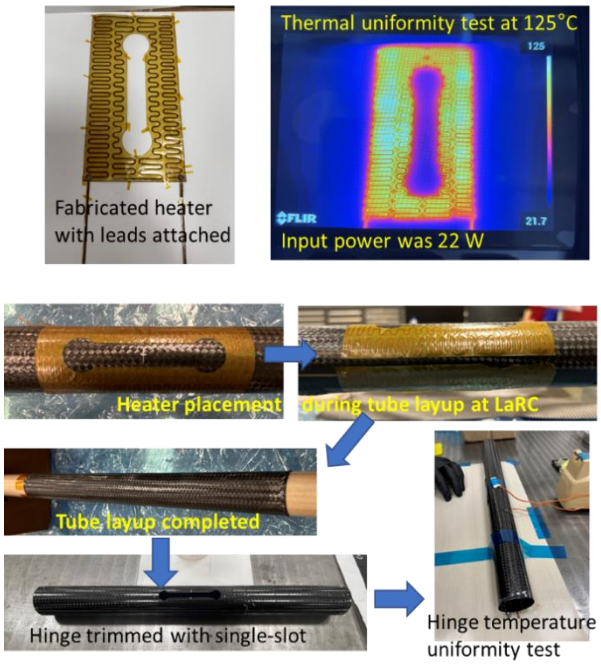

Fig. 11. Custom ultrathin-film heater produced by PSU and steps in the fabrication process of the SMC hinges with the embedded heaters. Temperature uniformity tests are carried out before and after integration of the heaters in the hinge.

The hexagonal rigid panels that form the reflective surface of the reflector are designed using a sandwich approach to yield a high specific stiffness construction. The 12.7-mm thick core was first machined from carbon foam (CFOAM 30®), which has density of 480 kg/m^3 and a CTE of 5 µm/(m·K) at temperatures above 200ºC. This is of the same order of magnitude of the carbon fiber reinforced plastic (CFRP) face sheets that are bonded to it, incurring in minimal thermal expansion mismatch. The machined foam cores were sealed with ES-215 epoxy resin mixed with IHG hardener that is used in high temperature composite tooling. The two panel cores are shown in Fig. 12. The 0.16-mm thick CFRP face sheets are co-cured directly onto the cores and bonded in a single step using a thin EA9696 epoxy film adhesive. The face sheet is a four-ply balanced and symmetric plain weave laminate with the thinnest design possible to ensure that dimpling on the core would not be a problem for high accuracy applications. Each hexagonal panel has a mass of ~6.4 kg with 85% of its mass being the core. A good rule of thumb to maintain adequate hexagonal sandwich panel stiffness is to make the core thickness proportional to the panel width (corner to corner) [4]. The machined core thickness of 12.7 mm could be reduced further but was not chosen for the two-panel assembly breadboard demonstrator to maintain panel precision during manufacturing and during thermal loading. A total sub-reflector mass at the 3.3-m scale of 57 kg would be expected, including backbone hardware, but assuming half of the thickness of the core would result in a total mass saving of 33%.

(a) (b)

Fig. 12. 1-m-wide hexagonal panel cores fabricated. (a) Backside of the side panel; (b) reflective side of the central panel.

The assembly of the final hardware is currently ongoing. The final test campaign will be carried out inside a thermal chamber at 80ºC. The test configuration will have the central hexagonal panel fixed with the convex side up on a pedestal and the side hexagonal panel stowed on top of it with the concave reflective side up. The two panels will be connected by a pair of two-slot SMC hinges corresponding to Side Panel #2 and a secondary locking mechanism. The mass of the side panel assembly including the backbone hardware attachment is 8.3 kg. The side panel will be supported by a semi-hexagonal frame that allows free rotation of the panel on bearings about the axis connecting two of its opposing corners as needed for the panel to swing open and end with the concave side down. The semi-hexagonal frame hangs from a pulley system that travels lengthwise in the thermal chamber using a trolley riding on an overhead conveyor track. The weight of the panel assembly will be offloaded by the hanging mass on the other end of the two-pulley system. The test configuration inside the thermal chamber is shown in Fig. 13.

Shape measurements of the reflective solid surface from three-dimensional scans of the test articles pre-and-post-deployment inside a thermal chamber will be used to assess the feasibility of this design architecture to support S-band and above radio frequencies (≥ 4 GHz) for large-scale antenna reflector applications. The goal is to demonstrate with the subscale breadboard model that the novel key features of the reflector that would be used in the designs at the 10-m scale and above are effective to enable efficient stowage with minimal constrains, controlled deployment, and maintain the necessary shape accuracy in space of < 3 mm root mean square (rms) error.

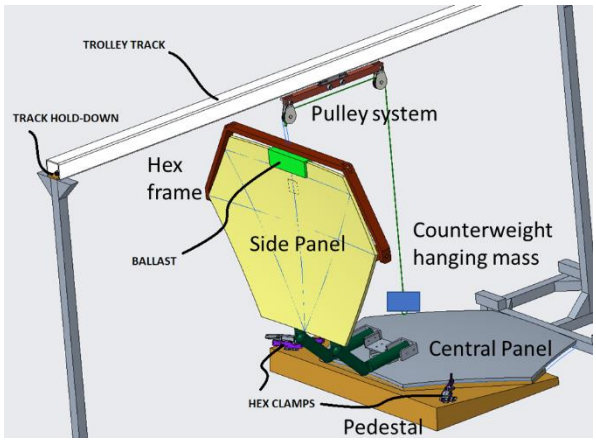

(a)

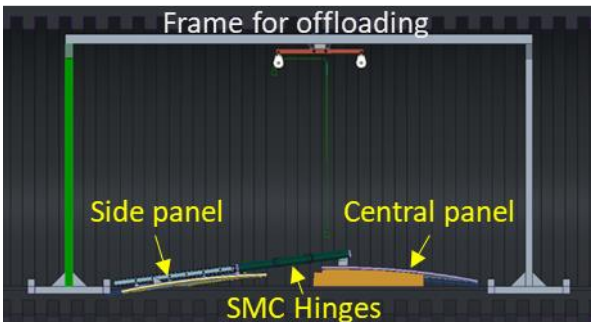

(b)

Fig. 13. Test configuration of the 3.3-m diameter scale two-panel assembly inside the thermal chamber for final validation of the system. (a) snapshot during the deployment phase showing the side panel in a vertical state; (b) final state of deployment of the tubular hinges prior to actuation of the secondary locking mechanism to close the panel-to-panel gap.

V. REFERENCES

[1] M. M. Mikulas Jr., P. R. Withnell, "Construction concepts for precision segmented reflectors," AIAA Paper 93-1461, 1993.

[2] B. B. Allen, C. F. Willer, R. I. Harless, R. V. Valentin, R. S. Sorrell, "Compactly stowable thin continuous surface-based antenna having radial and perimeter stiffeners that deploy and maintain antenna surface in prescribed surface geometry," U.S. Patent 6,344,835 B1, Issued 5 February 2002.

[3] J. Footdale, J. Cody Griffe, M. E. Peterson, and C. Box, "Flexible composite shell design for the MARCO deployable reflector," *AIAA Scitech 2019 Forum*, 7-11 January 2019, San Diego, CA.

[4] M. M. Mikulas Jr., T. J. Collins, J. M. Hedgepeth, "Preliminary design approach for large high precision segmented reflectors," NASA Technical Memorandum 102605, 1990.

[5] Y. She, S. Li, Z. Wang, "Constructing a large antenna reflector via spacecraft formation flying and reconfiguration control," *AIAA Journal of Guidance, Control, and Dynamics*, Vol. 42, No. 6, June 2019.

[6] NASA, *https://www.nasa.gov/press-release/nasa-funds-demonstration-of-assembly-and-manufacturing-in-space*, published Jan. 31, 2020.

[7] J. M. Fernandez, J. H. Kang, "Shape memory polymer composite substrate," U.S. Patent Application 63/452,712 filed on March 17, 2023.

[8] J. M. Fernandez, A. F. Paddock, K. Demarco, "Composite substrate reflector design," U.S. Patent Application 63/452,713 filed on March 17, 2023.

[9] H. M. Y. C. Mallikarachchi, S. Pellegrino, "Optimized design of composite booms with integrated tape-spring hinges," AIAA 2010-2750.

[10] D. S. Adams, M. Mobrem, "Lenticular jointed antenna deployment anomaly and resolution onboard the Mars Express spacecraft," AIAA Journal of Spacecraft and Rockets, Vol. 46, No. 2, pp. 403-410, March-April 2009.